Indian Journal of Engineering & Materials Sciences
Vol. 31, December 2024, pp. 812-825
DOI: 10.56042/ijems.v31i6.11937

Optimization of operating parameters of multi-lamp in-duct ultraviolet-c air disinfection system through computational fluid dynamics analysis

Monia Purnima Sharma *

Department of Physics, Dr. B R Ambedkar National Institute of Technology Jalandhar, Punjab 144 011, India

Received: 20 June 2024; accepted: 08 November 2024

This research has focused on optimizing operating parameters of a multi-lamp In-duct UVC air disinfection system through Computational Fluid Dynamics (CFD) analysis. The efficacy of the system has highly dependent on proper system design to ensure both effective disinfection and minimal energy consumption. In this study five configurations with varying numbers of Ultraviolet-C (UVC) lamps (3, 6, 9, 11, 13) of wavelength 254nm has been investigated through CFD analysis. The velocity and irradiation profiles corresponding to different lamp configurations has been studied to optimize number of lamps. Further orientation profile has been explored at the original vertical position, 30-degree rotation, 60-degree rotation, and horizontal position to optimize position of lamps within duct. The 13 lamps arrangement yields maximum germicidal action has been evidenced from velocity and irradiation profiles. The orientation profiles has revealed that a uniform vertical arrangement of lamps offers best position for achieving the maximum UV dose. Standard deviation calculations for UV dose distribution across different orientation positions has confirmed that a vertical arrangement provide an uniform dose distribution. In comparision to earlier studies, optimized 13-lamp configuration has resulted in a more than 60% increase in average uv dose, superior dose uniformity, and higher germicidal efficacy than conventional configurations.

Keywords: Germicidal efficacy, Irradiation profile, UV dose, UV dose distribution, Velocity profile

1 Introduction

In the pursuit of maintaining a healthy indoor environment, the adoption of air quality enhancement technologies has become imperative. Ultraviolet germicidal irradiation (UVGI) technologies have emerged out as effective measures for inactivating microorganisms, leveraging the power of ultraviolet-C radiation. These technologies have particularly applied in in-duct systems to mitigate the risk of airborne diseases within indoor environments[1]. The core of UVGI systems have laid in the deployment of multiple bare ultraviolet lamps strategically placed within the ducts of Heating, Ventilation, and Air-Conditioning (HVAC) systems, either wall-mounted or suspended from the ceiling[2]. These systems have utilized parallel louvers to direct UV light upward, creating a UV irradiation zone with elevated irradiance levels, commonly known as the UV zone [3]. The effectiveness of UVGI systems have predominantly attributed to the UV-C radiation wavelength band, particularly around 254 nm, which efficiently reduces microbial DNA[4]. Despite the proven efficacy of In-Duct UVGI (ID-UVGI) systems in air disinfection, there has been existed a gap in understanding their design and optimization. The factors that have contributed to this knowledge gap include a low awareness of microbial UV dose-response behavior, insufficient characterization of UV lamps, limited evaluations of energy consumption in UVGI systems, and uncertainties in inactivation performance[5]. Previous studies have identified key parameters influencing the performance of UVGI systems, including location, duct geometry, wavelength, relative humidity, lamp aspect ratio, temperature, reflectivity, and dose[6,7] . These studies have examined various UVGI systems and configurations but concentrated mostly on single or few-lamp arrays, simplified geometries, and reduced-order airflow simulations. In a study, UV dose calculation for single configuration have been done but no worthwhile insight have developed for how different comprehensive lamp configurations and orientation modifications affect dose uniformity and pathogen inactivation across the full cross-section of the duct[8]. Another study that has expanded the scope of analysis by systematically evaluating multiple lamp configurations and orientations, with a focus on dose uniformity and practical scalability[5]. This paper has focused on creating a more detailed and scalable framework for enhancing design in in-duct UVC air

*Corresponding author (E-mail: sharma.monia2011@gmail.com)

disinfection. It has incorporated insight into practical and energy-efficient configurations that ensure effective pathogen control, while offering data-driven recommendations through the study of the optimization of lamp arrangement as well as orientation to inform both optimal and even distribution of the UVC dose through improved air quality in variable indoor environments. The present research has systematically varied the counts, positions, and orientations of lamps in a controlled duct environment to study differences in ensuing airflow patterns and irradiation profiles with a greater level of detail than has not conducted in earlier studies. This integrated approach has determined the preferred configuration for increased disinfective germicidal efficacy, not only in terms of average UV dose but also in terms of its spatial distribution and influence of the retention time on the disinfection performance of particles. Compared to the generalized EPA guidelines followed by most of the studies related to the pathogen inactivation with indoor ventilation systems, this study has worked on tailoring the requirements of duct parameters, the position of UVC lamps, and material properties to enhance the performance of pathogen inactivation. This paper has aimed to bridge the existing gaps in understanding ID-UVGI systems by investigating the impact of varying configurations of UVC lamps (3, 6, 9, 11, 13) on system performance through CFD analysis. This study has systematically explored different lamp orientations (vertical, 30°, 60°, and horizontal at 90°) to determine their impact on UV dose distribution and air particle exposure. Understanding the role of lamp orientation is particularly crucial for retrofitting existing HVAC systems, where space constraints may limit the optimal placement of lamps. This study have fulfilled two objectives: The first one is to assess how different lamp orientations affect UV dose distribution within a duct and second one is to translate these differences into estimated inactivation efficiencies for common airborne pathogens, such as MS2 bacteriophage, SARS-CoV-2, and influenza virus, to provide actionable insights for optimizing UVGI system designs.

2 Materials and Methods

The proposed methodology for optimizing in-duct air disinfection systems through CFD analysis is a systematic and comprehensive approach, divided into multiple subsections to address critical aspects of system enhancement.

2.1 Duct configuration description

The geometry of the current simulation is considered by taking into account the parameters of EPA standards[9] as shown in Fig. 1. The cross-section area of the duct is 0.61 m x 0.61 m and the length of 1.83 metre total is given in Table 1. While the duct length in this study (1.83 m) deviates from the longer working lengths specified in EPA[9] and ANSI/ASHRAE standards, this choice reflects the need to evaluate compact systems applicable to constrained HVAC environments. The results, therefore, represent a conservative assessment, with anticipated enhancements in dose uniformity and particle retention in longer ducts. The average velocity of the air which enters the ventilation duct is 2.5 m/s. The UVC lamps used in this study have a nominal total power of 11 W and a UV-C output of 2.6 W at 254 nm, with a diameter of 1.9 cm. In contrast, the EPA standards[9] utilized four 25W lamps with a UVC output of approximately 8.5W each and a diameter of 1.9 cm. These differences in lamp specifications were taken into account during simulation to ensure accurate modeling of UV dose distribution. Unlike the 25 W lamps used in the EPA standards, our lamps reflect lower power configurations suitable for energy-efficient applications. The ballasts were matched to the lamps to ensure consistent performance, with lamp

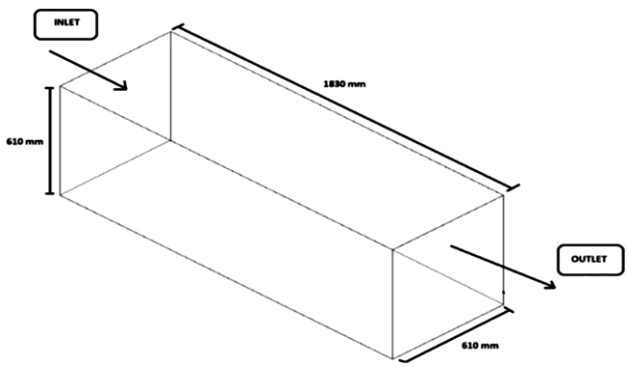

Fig. 1 — Geometry of grid.

Table 1 — Specification of induct UVC disinfection system.

Specification	600/R-06/051	Current simulation
Total number of lamps used	4	13
Total power of each lamp	25	11 watt
UVC power of each Lamp	8.5	2.6 watt
Total power of the system	100 watt	143 watt
Total UVC power of the system	34 watt	34 watt (approx.)
Length of each lamp	53.82cm	22.63 cm
Diameter of each lamp	1.9 cm	1.9 cm
Duct area	61cm×61cm	61 cm×61cm
Duct wall refractive index	1	1

characteristics validated using manufacturer specifications. A structured mesh has been created by using ANSYS meshing tools which contains 955K elements & refined close to the lamps. The mesh quality is explained in the result section. Five different configurations (3, 6, 9, 11, 13) of UVC lamps having an even distribution in the vertical position at the centre of duct has been studied in the current simulation. Three other lamp array configurations has been studied excluding the original vertical configuration. The original position has been marked as the main configuration & other positions are obtained by rotating original one through 30 degrees in counterclockwise direction. For all cases, distance between lamps is kept constant & rotation centre is considered as centre of lamps array. As the angle of rotation increases, a horizontal configuration of the lamp array is obtained.

2.2 Computational model description

The model for the UV-Disinfection duct system was created in Solid works 18 and then it was imported into ANSYS(18.2) Design Modeller. In the Design Modeller, the fluid volume was extracted from the imported geometry of the duct with lamps and then the fluid volume was sliced into the number of bodies to make it sweepable so that a structured grid can be generated in the ANSYS Meshing application. The CFD model was then imported into the ANSYS Meshing software. The Computational fluid dynamic model was divided into a finite number of small elements in the ANSYS Meshing tool. When governing equation of flow i.e. non-linear partial differential equations (Navier-Stokes equation) is applied to these small elements they get converted into algebraic equations. These algebraic equations are solved simultaneously using an iterative solver to get unknown variables at the cell centroids. The values of the unknown at the cell faces are then interpolated using one of the face interpolation schemes.

2.3 Boundary conditions

There were two types of material, (air and stainless steel) considered for this simulation. The air was considered as fluid & stainless steel (SS) was considered as solid walls of the duct. The absorption cofficient (α_c) & refractive index(n) of (SS) has been fixed so that it matches the sterilisation wavelength of UVC light of 254 nm. The value of absorption coefficient & refractive index has been considered to be 99,338,898 m^{-1} and 1 respectively [10]. The EPA[9] study does not specify the refrectivity inside the UV chamber report. The wall reflectivity is effected by different types of wall materials, dirt or dust etc. In this paper the total CFD simulation has been performed at diffusive wall reflectivity of 0% (emissivity=1).The Flow inside the duct has been considered to be steady state, and isothermal & turbulence have been estimated by using the k-ε model with standard functions of duct walls for all the cases. The boundary conditions that has been set is mentioned in Table 2.

Table 2 — Boundary conditions.

Zone	Property	600/R-06/051	Current Simulation
Inlet	Turbulence intensity	10	10
	Hydraulic Diameter	0.61	0.61
Duct walls	No Slip	-	-
	Diffusive Fraction	1	1
	emissivity	-	1
UV lamps	Direct irradiation ($W.m^{-2}$)	0	0
	Diffuse irradiation ($W.m^{-2}$)	294.17 per lamp* (Data from EPA)	535 per lamp
Outlet	UV Dose	-	30.24

2.4 CFD analysis of air disinfection system

There are four main sub processes of induct airdisinfection system: mathematical governing equations air flow modeling, UVC irradiation field modeling and particle tracking modelling. In order to better disinfect a detailed understanding of all these sub-processes is very important.

2.4.1Mathematical governing equations

In this research, the mathematical governing equations serve as the foundation for Computational Fluid Dynamics (CFD) analysis of the fluid flow and UVC disinfection process within a ventilation duct. These fundamental partial differential equations, applied to represent the characteristics of fluid flow, are solved algebraically at specified cells through meshing. These governing equations are rooted in conservative physics laws and include the conservation of mass, momentum conservation, and energy conservation.

2.4.2 Conservation of mass

The generalized form conservation of mass equation is represented by Eq. (1)[11]:

$$\frac{\partial \rho}{\partial t}+\nabla.(\rho \vec{v})=0 \quad \ldots (1)$$

The validity of this equation is for both incompressible as well as compressible flow. In Cartesian coordinate systems partial derivative form of Eq. (1) can be represented by Eq. (2):

$$\frac{\partial \rho}{\partial t}+\frac{\partial (\rho u)}{\partial x}+\frac{\partial (\rho v)}{\partial y}+\frac{\partial (\rho w)}{\partial z}=0 \quad \ldots (2)$$

where, velocity $\vec{v}$ in the flow field is expressed by local velocities u, v, & w, these are functions of position & time.

2.4.3 Momentum conservation equation

The momentum conservation is represented throughNavier-Stokes equation by Eq. (3):

$$\frac{\partial (\rho \vec{v})}{\partial t}+\nabla.(\rho \vec{v}\vec{v})=-\nabla \rho+\nabla.(\bar{\bar{\tau}})+\rho \vec{g}+\vec{F} \quad \ldots (3)$$

Where ρ, $\rho\vec{g}$, $\vec{F}$, $\bar{\bar{\tau}}$ is the static pressure, external forces, gravitational body force and the stress tensor respectively.

2.4.4 Energy equation

Energy conservation Eq. comes from thermodynamics first law:

$Time\ rate\ of\ change\ of\ energy = Net\ rate\ of\ heat\ added\ (\Sigma Q) + Net\ rate\ of\ work\ done\ (\Sigma W)$

By keeping the momentum Eq. into consideration the energy conservation can be described by Eq. (4)

$$\nabla.\left((\rho C_p)\vec{u}T\right) = \nabla.(k\nabla T) \quad \ldots (4)$$

In the energy equation, the left hand side term represents the convection of energy due to velocity and the right hand side term represents diffusion of energy.

2.4.5 Airflow model

One of the most important pre-requisites for a successful computational simulation is the ability to accurately estimate the distribution of airflow. . The presence of UVGI lamps within the duct creates localized turbulence, resulting in velocity fluctuations in both the axial and cross-sectional planes. This turbulence enhances particle mixing and increases UV-C exposure, without violating the conservation of mass, as the total volumetric flow rate remains constant. The k-ε turbulence model was used to simulate these effects and capture the complex flow behavior around the lamps. Reynolds averaged Navier-Stokes equations (represented by Eq. 5) & k-epsilon turbulence model are employed to provide solution for problem of airflow through ventilation duct. "In order to study the air flow pattern for ventilation application the k- epsilon model is exclusively used[12-15].The governing equations of flow is solved by ANSYS Fluent software with the FVM which divide computational domain into spatial elements. When attempting to estimate the turbulent energy and dissipation rate, the second order upwind approach is used. The modeling near walls of duct is performed with standard wall function. For all equations the values of convergence is 10^{-6}. The air which is supplied at duct's inlet is defined with boundary conditions of velocity inlet. At duct's outlet, the boundary condition for outflow is specified. In addition to this there is boundary condition of no slip is considered for all solid surfaces.

$$\frac{\partial (\rho \varphi)}{\partial t} + \nabla(\rho \varphi \overrightarrow{V}) = \nabla(\tau \varphi \nabla \varphi) + S\varphi \quad \ldots (5)$$

Where $\rho, \varphi, \vec{V}, \tau\varphi$ and $S\varphi$ represents density of air, independent variable, air velocity vector, source term & effective diffusive coefficient, respectively.

2.4.6 UVC irradiation field modelling

The discrete ordinates approach (DO) are employed to calculate irradiation field of a UVC lamps[16-17]. The discrete ordinate approach has also been used to solve the radiative transfer Eq. (RTE) represented by Eq. 6 for a finite number of discrete solid angles. This model will make it feasible to incorporate UV light reflection and refraction into the design. The user defines the parameters such as material characteristics, output of lamps & angular discretization within Fluent DO model (ANSYS 18.2). The irradiation distribution inside numerical model is defined by angular discretization, which is an essential factor.[31] The variation of irradiation distribution is based on mesh & two parameters $(\theta\ ,\ \emptyset)$,which specify discrete solid angles; more the angular divisions, more even will be resulting irradiation field, even though average irradiation will remain constant. Air has been considered as fluid &stainless steel (SS) as walls of duct for simulation. Internal emissivity of the material is what accounts for reflection in RTE model. In other words, a surface that produces reflections works as source of radiation emitting power in relationship to material's light absorption & energy it absorbs. The system's irradiation field is then expanded by this additional radiation. Due to the monochromatic nature of UVC lamps , there is no frequency influence that is taken into consideration. Since the amount of light scattered by suspended particles is negligible in comparison to the volume of air, it is assumed that the air is a homogenous medium.

$$\nabla.(I_\lambda(\vec{r},\vec{s})\ \vec{s}) + (\alpha_\lambda + \sigma_s)\ I_\lambda(\vec{r},\vec{s}) = \alpha_\lambda + \eta^2 I_{b\lambda} + \sigma_s/4\pi \int_0^{4\pi} I\lambda\left(\vec{r},\overrightarrow{s'}\right) \phi(\vec{s},\overrightarrow{s'})\ d\Omega \quad \ldots (6)$$

In the above equation, $\vec{r}$ is the position vector, $\vec{s}$ is scattering direction vector ,s represents the path length, $\alpha_\lambda$is coefficient of spectral absorption, n is refractive index, σ_s is scattering coefficient, $I_{b\lambda}$ is intensity of black body, $I\lambda$is intensity of radiation, λ is wavelength of UV light, ϕ is phase function& Ω is solid angle.

2.4.7 Particle motion model

The pathogen carriers' paths were investigated using discrete phase modeling (DPM) on a flow map that was created after assessing the flow of air. Depending on the Lagrangian reference frame, each pathogenic particle's trajectory is determined. The generalized form of the equation of discrete phase model is represented as equation (7):

$$du_p/dt = F_D (u-u_p) + g (\rho_p-\rho)/ \rho_p + F_a \quad \dots (7)$$

In the above equation, u, u_p represents the velocity vector of the air & pathogenic particle, respectively.ρ_p, ρ is the density of particles & air respectively. t is time and g is the gravitational acceleration, du_p/dt& $F_D (u-u_p)$ represent the inertial & drag forces, respectively. The last term F_a denotes additional forces such as the thermophoretic force, Saffman's lift force, Brownian force.

The impact of turbulence on particle distribution is examined using the discrete random walk model. This model predicts particle turbulence distribution by integrating direction equations for each particle by following Gaussian probability distribution of fluctuating velocities. The fluctuating velocity components u be calculated by using equation (8).

$$U'=\xi\sqrt{2k/3} \quad \dots (8)$$

In the above equation k, ξ are turbulent kinetic energy& normally distributed random number respectively.

The particle trajectory is determined by using the boundary conditions given in Table 2.There is the injection of pathogenic particles at the inlet of the duct. When the particles leave the duct and reach the outlet, the escape boundary condition is considered. Each pathogenic particle is considered in spherical shape &an average diameter& density of 1 μm&1000 kg/m^3respectively. This particle size is of specific interest for indoor air quality because it easily penetrates the respiratory tract[18]. The averaged no. of particles that has been tracked are in between 10,000 - 15,000 in each simulation.

2.4.8 UV dose calculations

The UV dosage absorbed by every particle in the computational domain is computed after particle trajectory simulation. The cumulative UV exposure was calculated using a user-defined function (UDF).The implemented algorithm calculates the lifetime UV dosage received by each particle. The formula for calculating the dosage is expressed in equation (9):

$$\text{UV Dose}=dt*\sum_{i=1}^{i=n}\frac{UV_i+UV_{i+1}}{2} \quad \dots (9)$$

In starting and end of the time steps, the values of and represent the UV irradiance, respectively. Additionally, an arithmetic mean may be used to drive the average UVC dosage of the tracked particle system by using equation (10).

$$\text{Average UVC dose} = \sum UVdose / n \quad \dots (10)$$

Further the disinfection performance of a system is based on a specific microorganism and the average dose which can be calculated by using equation (11):

$$S= ^{-Z.D} \quad \dots (11)$$

In the above equation S, Z represents the survival fraction, susceptibility of the microbes respectively & D is the mean value of UVC dosage of the system[19].

3 Results

In this section, The quality of mesh which has been studied through grid independence test has been discussed. Further the velocity profile and irradiation profile for all lamp array configurations (3, 6, 9, 11, and 13) are given. The optimization of number of lamps within the duct and their orientation has been studied. The Average value of UVC dose for optimized no. of lamps has been calculated. UVC dose distributions within the duct has been discussed in detail in the last portion.

3.1 Grid independence test

A Structured Tetrahedron mesh has been created for defind geometry as per EPA[9] study by using ANSYS ICEM CFD software. Radiation gradients around the lamps has been effectively captured by employing the inflation layer. The other regions has a coarsened mesh for reducing the cost of computation. The size of smallest element is considered to be 1 mm. A grid independence test is performed for checking the quality of mesh with three resolutions of grid: 894 k (coarse), 955 k (medium) & 987 k (fine). The sensitivity of these three meshes has been

analysed on the basis of irradiation & average UV dose vlues given in Table 3. The difference in the results of medium& fine quality mesh is very less in terms of average value of irradiation & average UV dose values. Therefore medium size mesh (about 955k) has been considered to perform further simulations by taking into account the resolution accuracy, time & cost of computation. In the above-considered mesh type, the maximum skewness of the grid is 0.78.

Table 3 — Grid independence test results.

	Coarse Mesh	Medium Mesh	Fine Mesh
Cell number	894k	955k	987k
Average velocity of air (m/s)	2.5	2.5	2.5
Maximum velocity of air (m/s)	4	4	4
Average UV dose (J/m^2)	30.79	30.36	29.84
Maximum dose (J/m^2)	68.35	67.56	66.67
Average irradiation (W/m^2)	43.6	44	44.12
Maximum irradiation (W/m^2)	1791	1795	1798

3.2 Velocity contour

The investigation of velocity contours in a vertical plane intersecting the duct's center for various lamp array configurations revealed crucial insights. The velocity profile was scrutinized in two distinct areas: the entrance, where the profile remained fully developed until encountering the disruption caused by the UVC lamps, and the exit, where alterations in airflow distribution were observed post the UVC lamp array. In all configurations (3, 6, 9, 11, 13 lamps), the presence of a boundary layer resulted in the lowest air velocity magnitudes near the duct walls and downstream of the UVC lamps. This reduced airflow velocity in these regions led to slower particle movement compared to other duct areas. Examining the 3-lamp configuration at the duct outlet highlighted lower velocities behind the lamp, indicating increased retention time for air particles in these region shown in Fig. 2. However, achieving the objective of affecting air particles with germicidal action proved unsuccessful, as particles reached the outlet with free stream velocity, emphasizing the need for adjustments. Increasing the number of lamps or reducing inter-spacing between lamps emerged as potential solutions to enhance retention time. Progressing to the 6-lamp configuration demonstrated improved results, with low-velocity zones superimposing and enhancing retention time. The subsequent 9-lamp configuration further optimized the setup, bringing low-velocity regions closer due to reduced inter-spacing, thereby increasing the efficacy of germicidal action. The 11-lamp configuration displayed heightened filtration efficiency and increased retention time compared to previous setups. However, the pinnacle of success was reached with the 13-lamp configuration, where the objective of passing all air particles through UV-C lamps for germicidal action and ensuring maximum retention time was achieved. Consequently, the 13-lamp configuration emerged as the optimized setup for effective germicidal action, as depicted in the Fig. 2. This detailed exploration of velocity contours and lamp configurations contributes valuable insights to the optimization of in-duct UVC air disinfection systems.

3.3 UV irradiation profile

The impact of the number of lamps on the UVC irradiation profile is illustrated in Fig. 3, encompassing configurations with 3, 6, 9, 11, and 13 lamps. Contours of the UVC irradiation field exhibit variability based on the lamp count, with higher irradiation intensity observed in proximity to the UVC lamps. The radial distance and circumference area play a pivotal role in irradiation values, showing a decrease as these parameters increase. Moving from a 3-lamp to a 13-lamp configuration, an observable increase in the irradiation area is noted.. The optimized 13-lamp arrangement ensures maximum germicidal action not simply by increasing lamp count, but through strategic spacing and orientation that minimize dark areas and maximize UV dose uniformity across airflow trajectories. The 13-lamp configuration stands out, demonstrating a minimal darker area, ensuring that irradiation extends to the duct's end, thereby facilitating enhanced germicidal action. The contours emphasize that the UVC dose rate hinges on the interplay between particle trajectories and irradiation fields. Optimal germicidal action is achieved when air particles closely interact with UVC lamps, indicating a correlation between dosage and lamp proximity.

3.4 Orientations profile

On the basis of findings from velocity and irradiation profiles that the 13-lamp configuration provides an optimal setup for germicidal action within the duct, the orientation profile of this configuration is

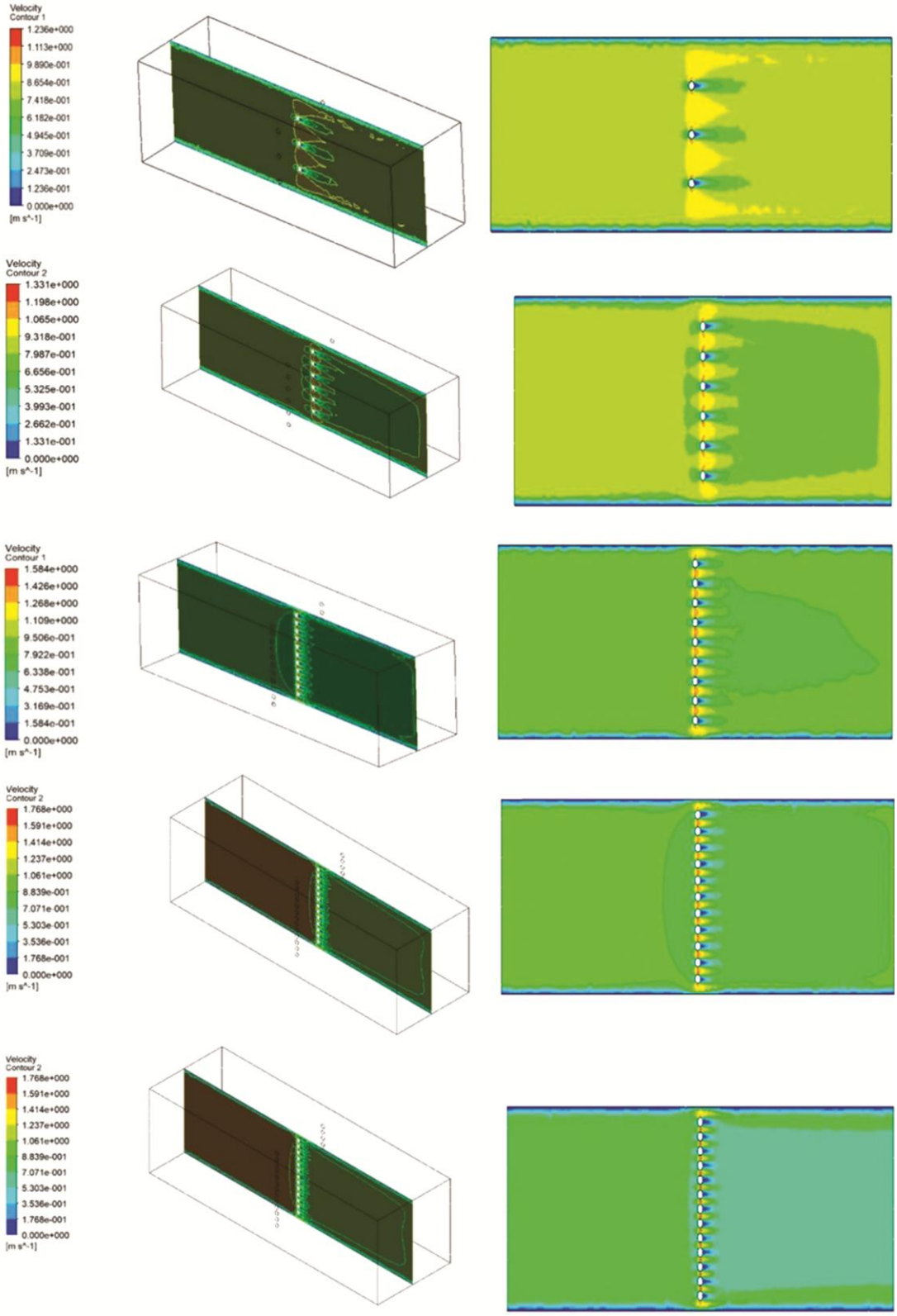

Fig. 2 — Velocity contour of 3,6,9,11,13 lamps arrangement.

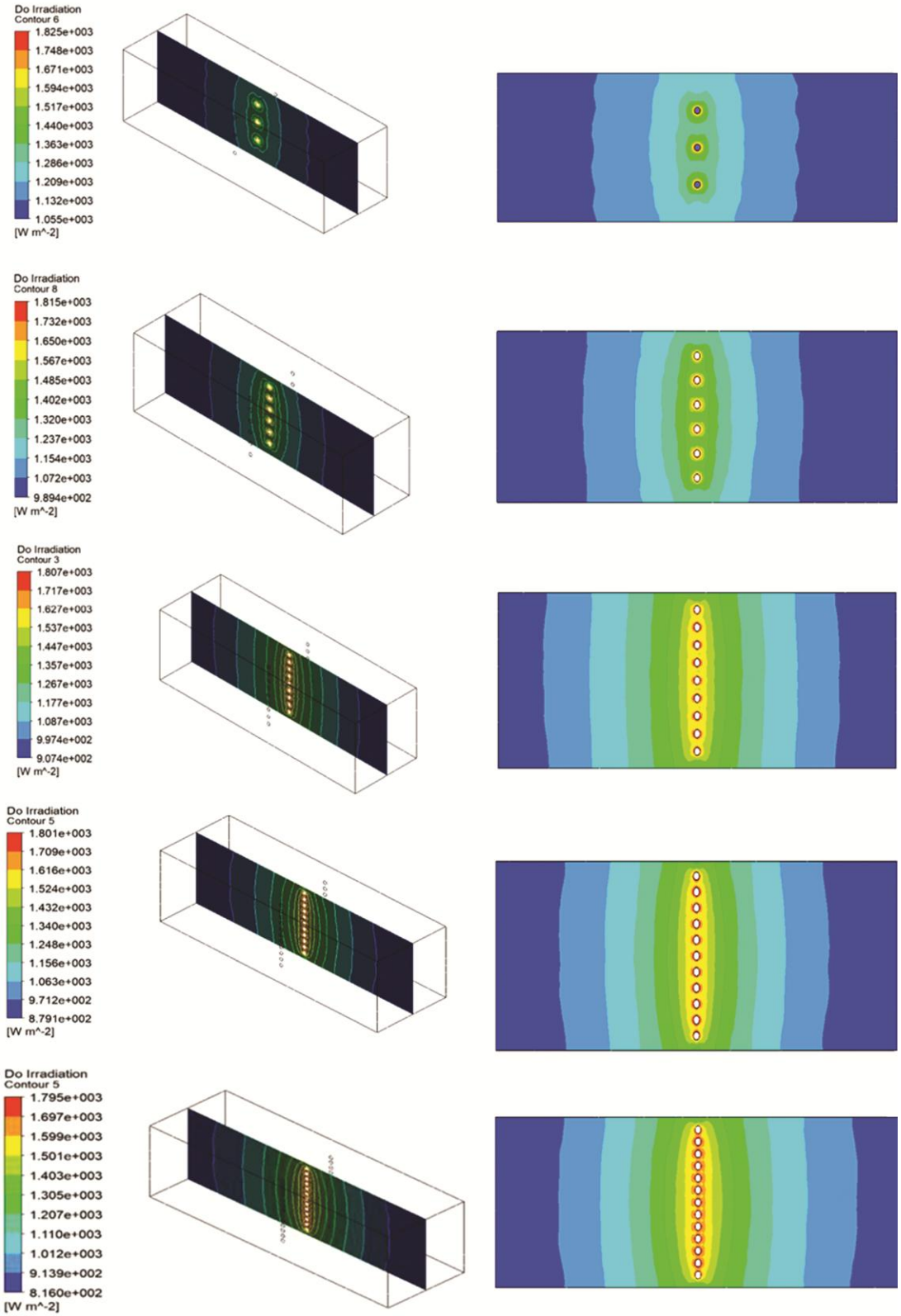

Fig. 3 — UV irradiation contours of 3,6,9,11,13 lamps arrangement.

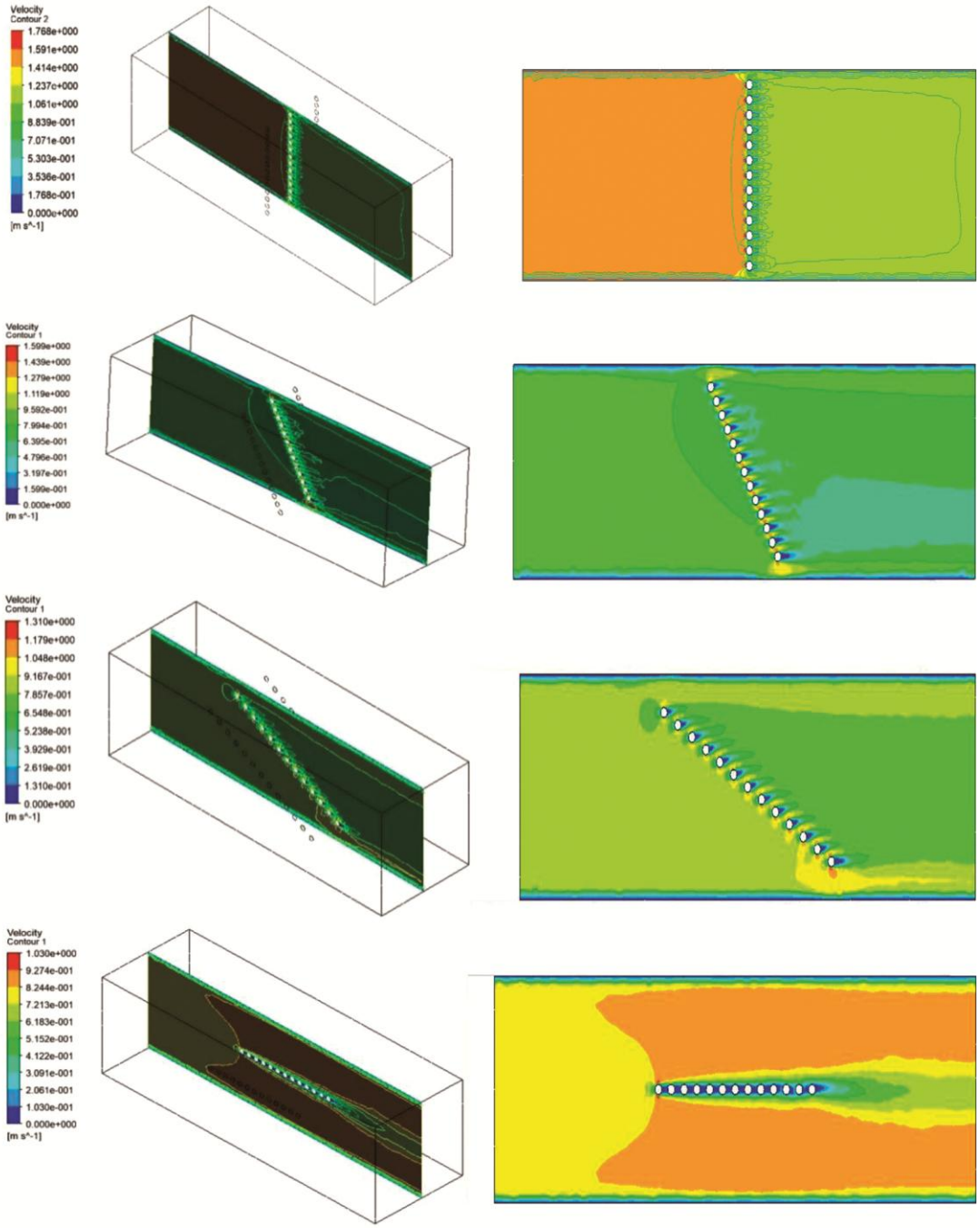

Fig. 4 — Velocity contour of 13 lamps arrangements at vertical , 30, 60, 90 degree of orientation.

explored in Fig. 4. Represented in the vertical position as the reference, the lamp array undergoes counterclockwise rotations at 30-degree intervals. A significant observation is made that the vertical position yields superimposed low-velocity regions, ensuring prolonged particle retention and efficient germicidal action. Conversely, at 30, 60, and 90-degree orientations, the velocity plots reveal air particles moving at free stream velocity at the outlet, indicating insufficient exposure to UV-C lamps for germicidal action.

3.5 UV dose calculation for 13 lamps arrangement

Post-simulation of particle trajectories, UVC doses received by each particle are computed, leading to the cumulative UVC dosage calculation. The average UVC dose, derived from the arithmetic mean of cumulative dosages for particles traversing the duct, increases with the number of lamps. For the 13-lamp

arrangement, the calculated UV dose is 30.24 $J.m^{-2}$ at 0% wall reflectivity which meets the threshold for effective germicidal action against the targeted pathogen as shown in Fig. 5. Subsequently, the disinfection rate for the target microbe, MS2 bacteriophage virus, is calculated based on the susceptibility values obtained from prior studies[20]. At a relative humidity range of 32–50%, the susceptibility value is 0.038 m^2/J, and for 74–82%, it is 0.048 m^2/J. The calculated average disinfection rate for MS2 bacteriophage is found to be 68.52%, affirming the effectiveness of the 13-lamp arrangement in achieving significant germicidal action within the duct. The calculated average disinfection rate for MS2 bacteriophage is approximately 68.5% ± 2.5%, reflecting the effectiveness of the 13-lamp configuration. A sensitivity analysis using susceptibility constants reported by study suggests that the disinfection rate may vary between 65% and 70% depending on specific environmental conditions[21].

3.6 Estimated inactivation efficiencies

To quantify the effect of different UV dose distributions, we estimated the inactivation rates of MS2 bacteriophage, SARS-CoV-2, and influenza virus using published UV susceptibility data as mentioned in Table 4. The UV dose-response models were applied to the average dose values obtained from our simulations to estimate the percentage of pathogens inactivated. The results indicate that while increasing the number of lamps generally improves the UV dose, optimizing lamp orientation can enhance the consistency of UV exposure. The vertical orientation (0°) consistently yielded higher inactivation rates compared to angled orientations, particularly in configurations with more lamps (9, 11, and 13).

3.6.1 Distribution of UVC dose

The average UVC dose for the 13-lamp arrangement provides an overall understanding, but the distribution among air particles passing through the duct necessitates a more in-depth exploration. Figure 6 depicts the UVC dose distribution for the 13-lamp configuration at various orientation positions (vertical, 30, 60, and 90 degrees), revealing distinct behaviors for each orientation.In both vertical and 30-degree orientations, three prominent UVC dosage peaks are evident, demonstrating values at 20.98 J/m²,

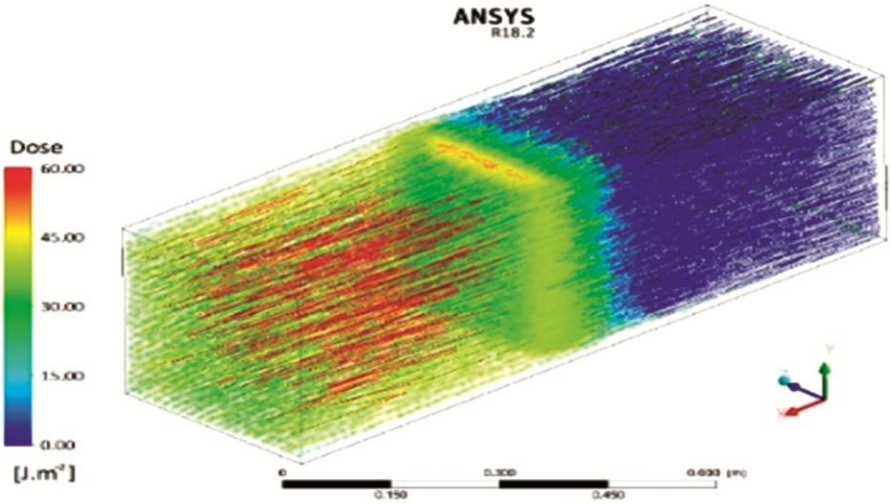

Fig. 5 — UVC dose value for 13 lamps arrangements.

Table 4 — Inactivation rates calculated using dose-response models derived from published data on pathogen susceptibility to UV-C irradiation.

Configuration Lamps	Average UV Dose (J/m²)	MS2 Inactivation (%)	SARS-CoV-2 Inactivation (%)	Influenza Inactivation(%)
3	18.5	45.3	38.7	40.1
6	21.9	56.7	49.8	52
9	25.4	62.1	55.3	58.4
11	28.3	66	59.7	63.1
13	30.24	68.5	63.2	66.4

26.47 J/m², and 34.12 J/m² in the vertical position, and at 22 J/m², 25.68 J/m², and 32.15 J/m² in the 30-degree orientation. The occurrence of UV dose peaks diminishes as the lamp configuration transitions towards a horizontal distribution (from vertical to 90-degree orientation). At 60-degree orientation, two small peaks and one prominent peak are observed, with UVC dosage values of 21.54 J/m², 29.35 J/m², and 32.81 J/m², respectively. In Case 4 (90-degree orientation), a single sharp UVC dose peak at 28.76 J/m² is observed. Despite the highest average UVC dosage being achieved at a 60-degree rotation, the non-uniform distribution of the irradiation field results in significant variations between high and low UVC dose readings. Further examination of UVC dose distribution is conducted in Fig. 7, which

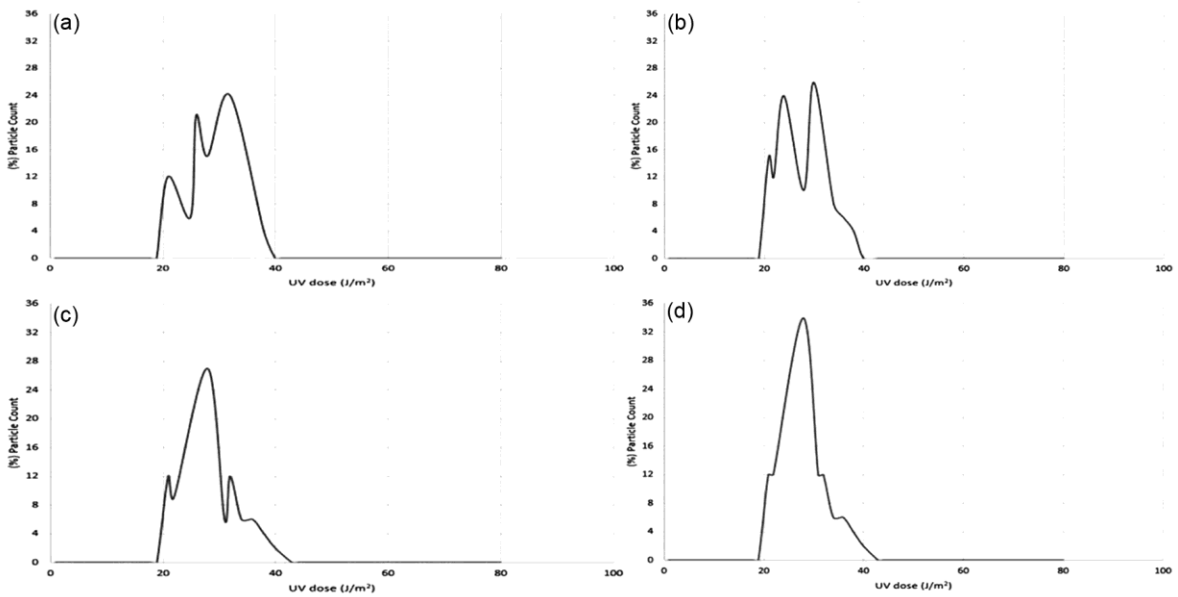

Fig. 6 — The distributions of UVC dose for 13 lamps arrangement in (a) vertical, (b) 30 degree, (c) 60 degree, and (d) 90 degree orientation positions.

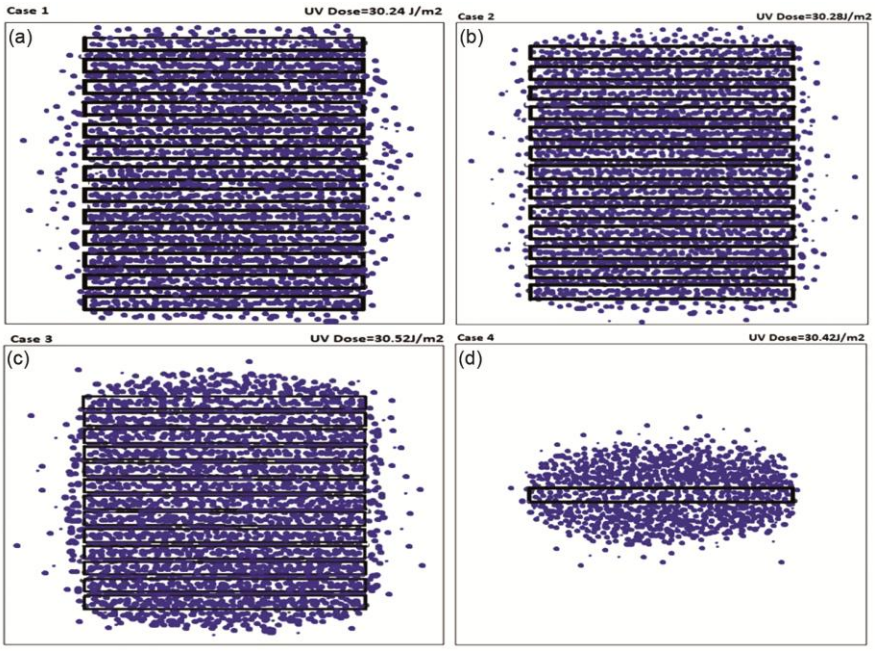

Fig. 7 — Cross-sectional view of outlet of the duct representing position of lamps.The average or more UVC dose received by particles; (a) Case 1 (>30.24 Jm^{-2}, 51%), (b) Case 2 (>30.28 Jm^{-2}, 49%), (c) Case 3(>30.52 Jm^{-2} 42.5%) and, (d) Case 4 (>30.42 Jm^{-2} 38.5%).

Table 5 — Values of standard deviation for each orientation configuration.

Configuration	The average value of UVC dose (J/m^2)	Standard deviation in UVC dose (J/m^2)	Standard deviation in UVC dose/average value of UVC dose (%)
Case 1	30.24	4.56	15.07
Case2	30.28	4.85	16.01
Case3	30.52	5.3	17.36
Case4	30.42	6.52	21.43

represents particles receiving greater than the average UVC dosage value at the system outlet. It is observed that particles exposed to higher-than-average UVC dosage values are concentrated in close proximity to the lamps. In the vertical position (Case 1), the widest spread is noted, with 51% of air particles obtaining greater than the average UVC dosage. Case 2 demonstrates that 49% of air particles received greater than the average UVC dosage. As the 13-lamp arrangement transitions to a horizontal configuration, the rate of particles receiving an overdose diminishes and occupies a smaller region. Case 3 indicates that 42.5% of particles received greater than the average UVC dosage value, while Case 4 exhibits the lowest overdose area, with only 38.5% of particles surpassing the average dosage value. Horizontal arrangements of 13 lamps, such as in Case 4, result in the most uneven distribution of UVC dose. In this scenario, air particles tend to concentrate near the top and bottom portions of the duct, receiving insufficient UVC dosage throughout their journey. Conversely, particles in close proximity to lamp areas receive a substantial UVC dose, contributing to an increased average rate. To holistically evaluate the in-duct UVC system, it is essential to consider both the average UVC dosage and its distribution. Therefore, standard deviation is introduced as an additional evaluation metric. A lower standard deviation indicates a more uniform distribution of UVC dose. The results in Table 5 reveal that, as the lamp array transitions from a vertical to a horizontal position, the standard deviation increases. Consequently, it is concluded that, among other performance parameters considered for the evaluation of the in-duct UVC system, the standard deviation of UVC dose distribution significantly contributes to an effective interpretation of system performance.

4 Discussion

This research paper explores the optimization of the number, position, oriention of lamps within a duct. But there is deviation of some parameters from EPA standards. The deviations are justified based on the specific requirements for optimizing in-duct UVC air disinfection systems, as follows:

The EPA standards do not prescribe exact lamp configurations or power densities for all setups, often assuming a generic layout. Here, the study explores specific lamp counts (3, 6, 9, 11, and 13) and orientations to determine optimal performance based on CFD outcomes. The 13-lamp configuration with specific power and spacing significantly enhances UV exposure, creating a more consistent dose across the airflow. This deviation allows the system to reach an ideal dose threshold across all particles, ensuring a higher inactivation rate. The manuscript employs a structured mesh refined around the lamps to simulate accurate radiation gradients, contrasting with EPA's standard assumptions, which may use coarser or less refined models. This choice was made to precisely capture irradiation behavior within the duct, leading to more accurate predictions of dose distribution and particle exposure. The high resolution allows for better control over dose uniformity, which is essential for systems targeting specific microbial reduction standards. By setting the refractive index at a value specific to 254 nm UV light, the study diverges from broader EPA models. This precise calibration allows the duct materials to better reflect UVC light's germicidal properties, ensuring more efficient use of irradiance and improved disinfection outcomes.

4.1 Comparison with previous studies

The comparison of current simulations work with previous studies[15,19] has shown in Table 6. Our findings differ from the study due to the unique geometry of our duct system and the use of multiple lamp orientations. A comparison with study[15] reveals that increasing lamps from three to thirteen, while maintaining the same duct dimensions and total UVC power, enhances average UV dose with a more uniform distribution, indicative of improved germicidal efficacy. This comprehensive analysis underscores the importance of lamp configuration, orientation, and distribution in achieving optimal germicidal action within duct systems, offering valuable insights for the design and implementation of UVC air disinfection systems.

Table 6 — The value of average UVC doses from reference studies.

Studies	Average UVC dosage ($J.m^{-2}$)
Kowalski et al. (2009)[21]	18
Capetillo et al. (2015)[34]	18.45
Present simulation work	30.24

In previous studies[15,19], longer ducts and standardized configurations were used, which resulted in less uniform airflow patterns and UV dose distribution. However, in our study, the shorter duct length and varied orientations introduced localized airflow distribution, which impacted the UV dose received by air particles. The vertical orientation provided the most uniform UV distribution, minimizing areas of low UV exposure, which is essential for achieving high inactivation rates. In contrast, the angled orientations (30°, 60°) led to uneven dose distributions, creating pockets where pathogens were not adequately exposed to UV light. This resulted in lower overall inactivation rates compared to the vertical orientation.

These findings have practical implications for the design and optimization of UVGI systems, particularly in retrofitting existing HVAC systems. By optimizing lamp orientation, system designers can achieve more effective pathogen inactivation without necessarily increasing the number of lamps or power consumption. The inactivation estimates for pathogens such as SARS-CoV-2 and influenza demonstrate that orientation adjustments can significantly improve the efficacy of UVGI systems, making them more cost-effective and energy-efficient.

5 Conclusion

In light of the escalating threat posed by hospital-acquired infections (HAIs) attributed to drug-resistant pathogens and the pervasive health risks posed by the COVID-19 virus, the focus on disinfection through UVGI systems has intensified. This study addresses the pressing need for effective infection control by employing CFD analysis, presenting a cost-effective and time-efficient alternative to traditional experimental methods for evaluating design parameters. The paper utilizes CFD analysis to assess the performance of an in-duct UVGI system, specifically examining five lamp array configurations (3, 6, 9, 11, 13). The results, meticulously scrutinized in terms of flow profile, irradiation profile, UV dose distribution, and lamp orientation, reveal compelling insights into the system's functionality. Notable findings emphasize the profound influence of the number and positioning of lamps on the UVC system's operation. While acknowledging the limitations of the current simulation, confined to a straight ventilation duct with centrally located lamps, the study suggests promising avenues for future research. Recommendations include exploring diverse lamp locations, configurations with multiple lamp columns, and variations in duct geometries, such as bends or contractions/expansions, to broaden the applicability of in-duct UVGI systems in ventilation applications.

Acknowledgments

The author is grateful to director of Dr. B.R. Ambedkar National institute of Technology, Jalandhar for providing necessary administrative support in conducting the present study. We would like to thank our colleagues specializing in HVAC systems, microbiology, and UV-C disinfection technology for their invaluable feedback on the airflow modeling, microbial inactivation parameters, and practical implementation of in-duct UVGI systems. Their contributions have significantly strengthened the quality of this study.

References

1 Al-Rawi M, Lazonby A & Smith C, *Hardware X*, 11 (2022) 1.
2 Yang Y, Zhang H, Chan V & Lai A C, *Build Environ*, 152 (2019) 160.
3 Berry G, Parsons A, Morgan M, Rickert J & Cho H, *Environ Res*, 203 (2022) 1.
4 Thatcher C H & Adams B R, *Chemi Engi Sci*, 230 (2021) 1.
5 Luo H & Zhong L, *Build Environ*, 197 (2021) 1.
6 Demeersseman N, Saegeman V, Cossey V, Devriese H & Schuermans A, *J Hospital Infect*, 132 (2023) 85.
7 Shrestha P, DeGraw J W, Zhang M & Liu X, *Build and Environ*, 206 (2021) 1.
8 Capetillo A, Noakes C J & Sleigh P A, *Sci Technol Built Environ*, 21 (2015) 45.
9 EPA. (2006c). Biological Inactivation Efficiency by HVAC In-Duct Ultraviolet Light Systems: Atlantic Ultraviolet Corp. Report Nr EPA 600/R-06/ 051. Las Vegas, NV: National Homeland Security Research Center, Office of Research and Development, U.S. Environmental Protection Agency.
10 Karlsson B & Ribbing C G, *J Appl Phys*, 53 (1982) 6340.
11 Tu J, Yeoh G H & Liu C, Computational Fluid Dynamics (Butterworth-Heinemann) (2007).
12 Launder B E & Spalding D B, *Comput Methods Appl Mech Eng*, 3 (1974) 269.
13 Gadgil A J, Lobscheid C, Abadie M O & Finlayson E U, *Atmosp Environ*, 37 (2003) 5577.

14 Zhang Z & Chen Q, *Atmosph Environ*, 40 (2006) 3396.
15 Capetillo A, Structure and Performance of In-Duct UV Air Sterilisation Systems, Ph.D. Thesis, School of Civil Engineering, The University of Leeds, 2015.
16 Ho C K , Radiation Dose Modeling in Fluent, Workshop Proceedings, University of North Carolina (2009).
17 Pareek VK & Adesina A A, *AIChE J*, 50 (2004) 1273.
18 Perez-Padilla R, Schilmann A& Riojas-Rodriguez H, *Int J Tuberculosis Lung Disease*, 14 (2010) 1079.
19 Kowalski W, Ultraviolet Germicidal Irradiation Handbook (Springer-Verlag, Berlin Heidelberg) (2009).
20 Walker CM & Ko G.P, *Environ Sci Technol*, 41 (2007) 5460.
21 Snelling W J, Afkhami A, Turkington H L, Carlisle C, Cosby S L, Hamilton JW & Dunlop P S, *J Aerosol Sci*, 164 (2022) 106003.